THE LOCATION OF CYTOCHROME *c* ON THE SURFACE OF ULTRATHIN LIPID MULTILAYER FILMS USING X-RAY DIFFRACTION

JAMES M. PACHENCE AND J. KENT BLASIE
Department of Chemistry, University of Pennsylvania, Philadelphia, Pennsylvania 19104

ABSTRACT X-ray diffraction and spectroscopic techniques were used to characterize ultrathin fatty acid multilayers having a bound surface layer of cytochrome *c*. Three to six monolayers of arachidic acid were deposited onto an alkylated glass surface, using the Langmuir-Blodgett method. These fatty acid multilayer films were stored either in a 1 mM $NaHCO_3$ pH 7.5 solution or a buffered 10 μM cytochrome *c* solution, pH 7.5. After washing extensively with buffer, these multilayer films were assayed for bound cytochrome *c* by optical spectroscopy. It was found that the cytochrome *c* bound only to the odd-numbered monolayer films (which have hydrophilic surfaces). The theoretical number of cytochrome *c* molecules bound to the ultrathin multilayer films having three or five monolayers was calculated as $N = 1.2 \times 10^{13}/cm^2$ (assuming a hexagonally close-packed monolayer of protein), which would produce an optical density of 0.002 at a wavelength of 550 nm; for a three or five monolayer ultrathin film that was incubated with cytochrome *c*, $OD_{550} \approx 0.002$. The protein was released from the film when treated with >100 mM KCl solution, as would be expected for an electrostatic interaction. Meridional x-ray diffraction data were collected from the arachidic acid films with and without a bound cytochrome *c* layer. A box refinement technique, previously shown to be effective in deriving the profile structures of nonperiodic ultrathin films, was used to determine the multilayer electron density profiles. The electron density profiles and their autocorrelation functions showed that bound cytochrome *c* resulted in an additional electron dense feature on the multilayer surface, consistent with a bound cytochrome *c* monolayer. The position of the bound protein relative to the multilayer surface was independent of the number of fatty acid monolayers in the multilayer. Future studies will use these methods to investigate the structures of membrane protein complexes bound directly to the surface of multilayer films.

INTRODUCTION

The determination of the structures of molecular components involved in biological electron transfer, and the investigation of their supramolecular organization, is fundamental to the understanding of cellular energy conversion (e.g., 1–4). The ability to isolate and subsequently reincorporate relatively pure membrane molecular components into lipid bilayers and monolayers has provided a novel technique to help elucidate the structure–function relationships of biological energy transducing components (e.g., 1–7). These reconstituted systems have been useful for determining the functional capabilities of membrane components (or their complexes), especially in the generation of transmembrane phenomena, primarily due to (*a*) the higher concentration of the components of interest, versus in situ membranes; (*b*) the experimental control over the number and stoichiometry of the membrane constituents; and (*c*) the fabrication of membranes with macroscopic in-plane dimensions (e.g., 6, 7).

Similarly, membrane structure studies have used reconstituted systems to take advantage of these characteristics, in combination with the ability to selectively label the various molecular components. For example, extensive x-ray and neutron diffraction studies were performed on thick, oriented membrane multilayers consisting of reconstituted membranes containing phosphatidylcholine and photosynthetic reaction center proteins from the bacterium *Rps. sphaeroides* (1, 8). As a consequence of these studies, the profile structure of the protein and its position relative to the lipid bilayer was derived (1, 8). Similar structural studies of cytochrome *c* bound to the reaction centers in these reconstituted membranes provided the position of the cytochrome *c* molecule relative to the reaction center molecule in the membrane profile (2); resonance x-ray scattering from these reconstituted cytochrome *c*/reaction center/phospholipid membrane multilayers also established the distance between the heme iron of cytochrome *c* and the iron coupled to quinone in the reaction center protein (3). However, the success of this work was a direct consequence of the fact that the reconstituted membrane preparation consisted of microscopic unilamellar vesicles in which the protein was essentially unidirectionally incorporated in the bilayer; this generally does not occur for reconstituted systems, especially for higher protein to lipid

ratios. With this limitation in mind (which seriously affects both structural and functional studies on reconstituted membrane systems), we have set out to develop a more general approach for the unidirectional reconstitution of membrane molecular components into lipid monolayer/bilayer systems having macroscopic in-plane dimensions.

In this paper, we report the initial development and structural studies of surface-active ultrathin multilayer films to study the structure and supramolecular organization of membrane-associated proteins. We chose to first study the electrostatic binding of cytochrome *c* to ultrathin multilayer films consisting of simple fatty acids as our model system, considering that cytochrome *c* type molecules participate in the electron transfer reactions in various prokaryotic and eukaryotic systems. In addition, cytochrome *c* interactions with lipid monolayer and bilayer systems have been extensively investigated (e.g., 9–12); in particular, it has been previously shown that cytochrome *c* strongly interacts with simple fatty acid monolayers, and that the binding of cytochrome *c* to a lipid film surface can be directly measured spectrophotometrically (12). Ultrathin multilayer films used in this study were created via the Langmuir-Blodgett method to produce finite sequences of three to six molecular monolayers of fatty acids (13); the films were deposited on planar alkylated glass slides, resulting in either a polar film surface (carboxyl groups) for the multilayers having an odd number of deposited monolayers, or a nonpolar film surface (methyl groups) for those having an even number of deposited monolayers. The amount of cytochrome *c* electrostatically bound to the surface of these multilayer films was determined via double-beam spectrophotometry. Furthermore, we have collected meridional x-ray diffraction (the elastic photon momentum transfer along the axis perpendicular to the substrate surface) for the ultrathin multilayers of three and five monolayers of fatty acid, with and without electrostatically bound cytochrome *c*, along with x-ray diffraction data from four and six monolayers of fatty acid. Previously, we have used novel methods in the analysis of the meridional x-ray diffraction data from finite, periodic (each monolayer of identical species), and nonperiodic sequence multilayer films containing from two to ten molecular monolayers (14, 15). These same methods have been used here to derive the electron density profile structure of these ultrathin multilayer films with or without bound cytochrome *c*.

MATERIALS AND METHODS

Flat glass plates ($11 \times 25 \times 1$ mm^3) were coated with octadecyltrichlorosilane (OTS; Aldrich Chemical Co., Milwaukee, WI), according to the method by J. Sagiv (16) to form a hydrophobic substrate surface. Arachidic acid (Aldrich Chemical Co.) was zone refined with 50 zone passes at a rate of 1 cm/h and the purity of the center fraction confirmed by differential scanning calorimetry (DSC) measurements (model 990; Dupont Co., Wilmington, DE). Type VI horse heart cytochrome *c* was obtained from Sigma Chemical Co. (St. Louis, MO).

Multilayer films of arachidic acid were deposited onto the alkylated glass substrates via the Langmuir-Blodgett technique, as described previously (14). A subphase consisting of 1 mM $CdCl_2$ solution was used in a Lauda Langmuir trough system; the arachidic acid monolayer was kept at a constant surface pressure of 20 dyn/cm and a temperature of 17.5°C during the deposition, with the pH monitored during deposition (pH 5.5 ± 0.2). The substrate was dipped through the monolayer at a rate of 0.3 cm/min. These deposition conditions "stabilize" the monolayer at the air/water interface and result in the deposition of the fatty acid itself (14, 15).[1-3] If an odd number of monolayers were to be deposited, a 10-ml glass vial was placed in the subphase directly below the dipping mechanism before forming the lipid monolayer on the subphase. The glass slide, being below the subphase on the last deposition of an odd number of monolayers, was released from the dipping mechanism directly into the glass vial. In this manner, the hydrophilic film surface was always in contact with the polar solvent. The glass vial was then placed into a 500-ml container of buffer (1 mM $NaHCO_3$ at pH 8) and allowed to equilibrate for 24 h. The cadmium-free buffer was changed twice over the next 24-h period.

Ultrathin multilayer films consisting of three to six monolayers of arachidic acid were incubated for 48 h or more in 10 μM cytochrome *c* solution in 1 mM $NaHCO_3$, pH 8. Each film was removed from the cytochrome *c* solution and incubated with 1 mM $NaHCO_3$ buffer for 2 h or more. The buffer was changed every 5 min until there was no detectable cytochrome *c* measured spectrophotometrically in the supernatant. The glass slide substrate supporting the ultrathin multilayer films was then resuspended in a quartz cuvette (1-cm path length), containing a solution of 1 mM $NaHCO_3$ and 0.1 mM Ascorbate (to reduce the cytochrome *c*) at pH 8, and the optical absorption spectra were recorded with a double beam spectrophotometer (2).

Meridional x-ray diffraction was obtained from the multilayers as a function of $q_z = (2 \sin \theta)/\lambda$, corresponding to elastic photon momentum transfer along the *z*-axis, perpendicular to the substrate plane. This meridional x-ray diffraction arises from the projection of the three-dimensional multilayer electron density distribution along radial vectors lying in the layer planes perpendicular to the *z*-axis onto the *z*-axis; the projection is defined as the electron density profile for the multilayer. The incident x-ray beam defines an angle omega (ω) with the substrate plane ($x - y$). Meridional x-ray diffraction is observed for ω equal to θ, where 2θ is the angle between the incident and scattered beams. The multilayers were therefore positioned on the ω axis of a two-axis Huber diffractometer, which was scanned over an appropriate range of values permitting the collection of meridional diffraction data with a low impedance position-sensitive detector (PSD) aligned along the q_z direction and mounted on the 2θ axis. An Elliott (GX-6) rotating anode x-ray generator was used to produce the incident Cu K_α x-rays at a target loading of ~2.5 KW/mm^2. K_α x-rays were selected with a nickel filter and line-focused at the PSD entrance window using Franks' optics, with the line focus parallel to the multilayer substrate plane. The odd-number monolayer multilayers with or without bound cytochrome *c* were placed in sealed canisters and equilibrated with an atmospheric relative humidity of 98% (using a saturated salt solution of K_2SO_4), and all samples were kept at room temperature during the experiment.

Details regarding diffraction instrumentation and omega scan parameters have been previously described (14, 15). Each omega scan required ~10 h, resulting in a composite pattern which represents the meridional intensity function $I(q_z)$. Each intensity function was corrected for background scattering followed by a Lorentz correction of q_z to correct for oscillation of the multilayers in the omega scan to yield the corrected intensity function $I_c(q_z)$.

[1]Fischetti, R., M. Filipkowski, A. Garito, and J. K. Blasie, manuscript submitted for publication.

[2]Fischetti, R., J. M. Pachence, and J. K. Blasie, manuscript submitted for publication.

[3]Fischetti, R., V. Skita, A. F. Garito, and J. K. Blasie, manuscript submitted for publication.

RESULTS

The optic absorption spectra from a three or five monolayer arachidic acid multilayer, preincubated with cytochrome *c* as outlined in Materials and Methods, were typical of reduced cytochrome *c* (Fig. 1 *A*). Cytochrome *c* spectra were not detected from four or six monolayer arachidic acid multilayers incubated with cytochrome *c*, which was also the case for those multilayers not incubated with the protein (similar to the spectrum of Fig. 1 *C*). Assuming that the cytochrome *c* molecule is roughly spherical, having a radius r of 15.5 Å, the number of molecules per cubic centimeter in a hexagonally close-packed monolayer would be $N = 10^{16}$ Å^2/cm^2/$2r^2\sqrt{3}$ Å^2 = 1.2×10^{13} cm^{-2}. As the molar extinction cytochrome *c* is ϵ = 19,500 M^{-1} cm^{-1} at 550 nm, then a hexagonally close-packed cytochrome *c* monolayer bound to the multilayers on both sides of the glass substrate would produce an OD of 0.002 at 550 nm. The optical density at 550 nm of Fig. 1 *A* is therefore approximately equal to that for a cytochrome *c* monolayer bound to the arachidic acid multilayer surface. Since the interaction between cytochrome *c* and the arachidic acid surface is mainly electrostatic, binding should be inhibited at high ionic strength. Therefore, the ultrathin multilayer films with bound cytochrome *c* were incubated with 0.1 M KCl for 24 h or more. After removing the glass slide with the multilayer film, the optical spectrum for the supernatant (reduced with ascorbate) was measured and is shown in Fig. 1 *B*. Little or no optical absorbance from cytochrome *c* remained on the washed multilayer film (Fig. 1 *C*).

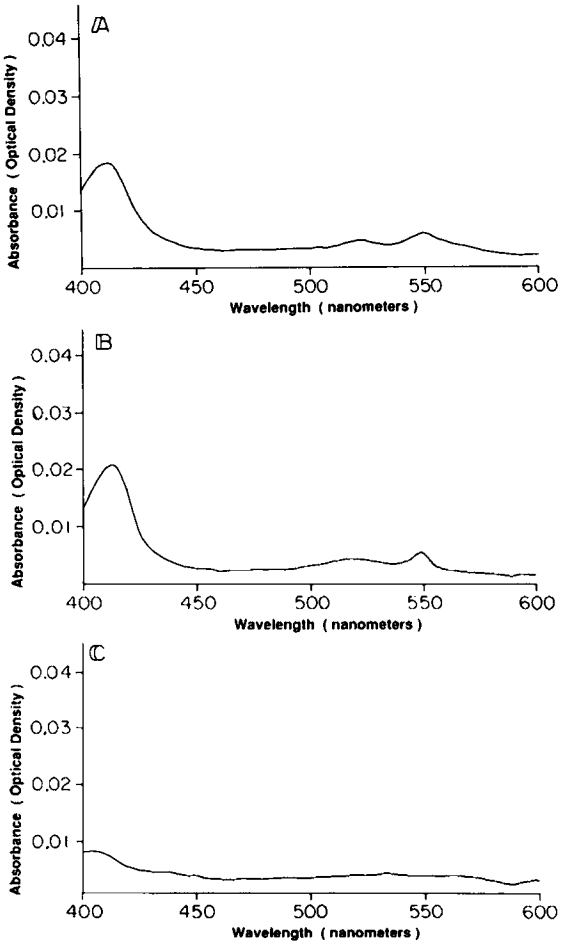

FIGURE 1 Optical absorption spectra of (*A*) cytochrome *c* bound electrostatically to the surface of an ultrathin multilayer substrate consisting of three monolayers of arachidic acid; (*B*) cytochrome *c* dissociated from the ultrathin multilayer substrate of *A*, using 100 mM KCl; (*C*) the ultrathin multilayer substrate of *A* after treatment with 100 mM KCl.

Meridional x-ray diffraction from two sets of ultrathin multilayer films were collected: Fig. 2 shows the corrected intensity data $I_c(q_z)$ for the ultrathin films having (*A*) three monlayers of arachidic acid (AAA), (*B*) three monolayers of arachidic acid with bound cytochrome *c* (AAA w/cyto), and (*C*) four monolayers of arachidic acid (AAAA). Fig. 3 shows $I_c(q_z)$ for (*A*) five monolayers of arachidic acid (AAAAA), (*B*) five monolayers of arachidic acid with bound cytochrome *c* (AAAAA w/cyto), and (*C*) 6 monolayers of arachidic acid (AAAAAA).

The corrected intensity functions of Figs. 2 and 3 are indicative of diffraction from asymmetric multilayer profiles of finite extent. Asymmetry is manifest primarily as non-zero minima between diffraction maxima, which is evident in each of the intensity functions of Figs. 2 and 3 (14); note, however, that the greatest amount of asymmetry is evident for the multilayers having an odd number of monolayers without bound cytochrome *c* (Figs. 2 *A* and 3 *A*). This result is as expected, for the multilayers having even numbers of monolayers exhibit inherently more symmetry in their intensity functions (see Figs. 2 *C* and 3 *C*) than the data from the three and five monolayer films. The intensity functions from multilayers having an odd number of monolayers with bound cytochrome *c* (Figs. 2 *B* and 3 *B*) exhibited an intermediate amount of asymmetry, as they can be viewed as having the same number of "layers" as the four and six monolayer films.

The broad resolved (in Δq_z) shape of the maxima and shifts in their positions (in q_z) from ℓ/d_0 (where d_0 is the profile extent of the average bilayer in the multilayer, and ℓ is an integer) result from the fact that the multilayer profiles are of limited extent (see Skita et al., 1986 for a full treatment of this phenomena). As expected, it was observed the diffraction maxima sharpen as the number of layers increase from three to six (compare Figs. 2 *A*, 2 *C*, 3 *A*, and 3 *C*).

The one-dimensional Fourier transform of the corrected meridional intensity function yields the autocorrelation function of the multilayer relative electron density profile, which requires no phase information. The autocorrelation function for each set of intensity data (Figs. 2 and 3) were calculated as shown in Figs. 4 and 5. These autocorrelation functions are approximately pseudoperiodic in d_0 and decay monotonically to zero with increasing $|z|$ for $|z| > D_n$,

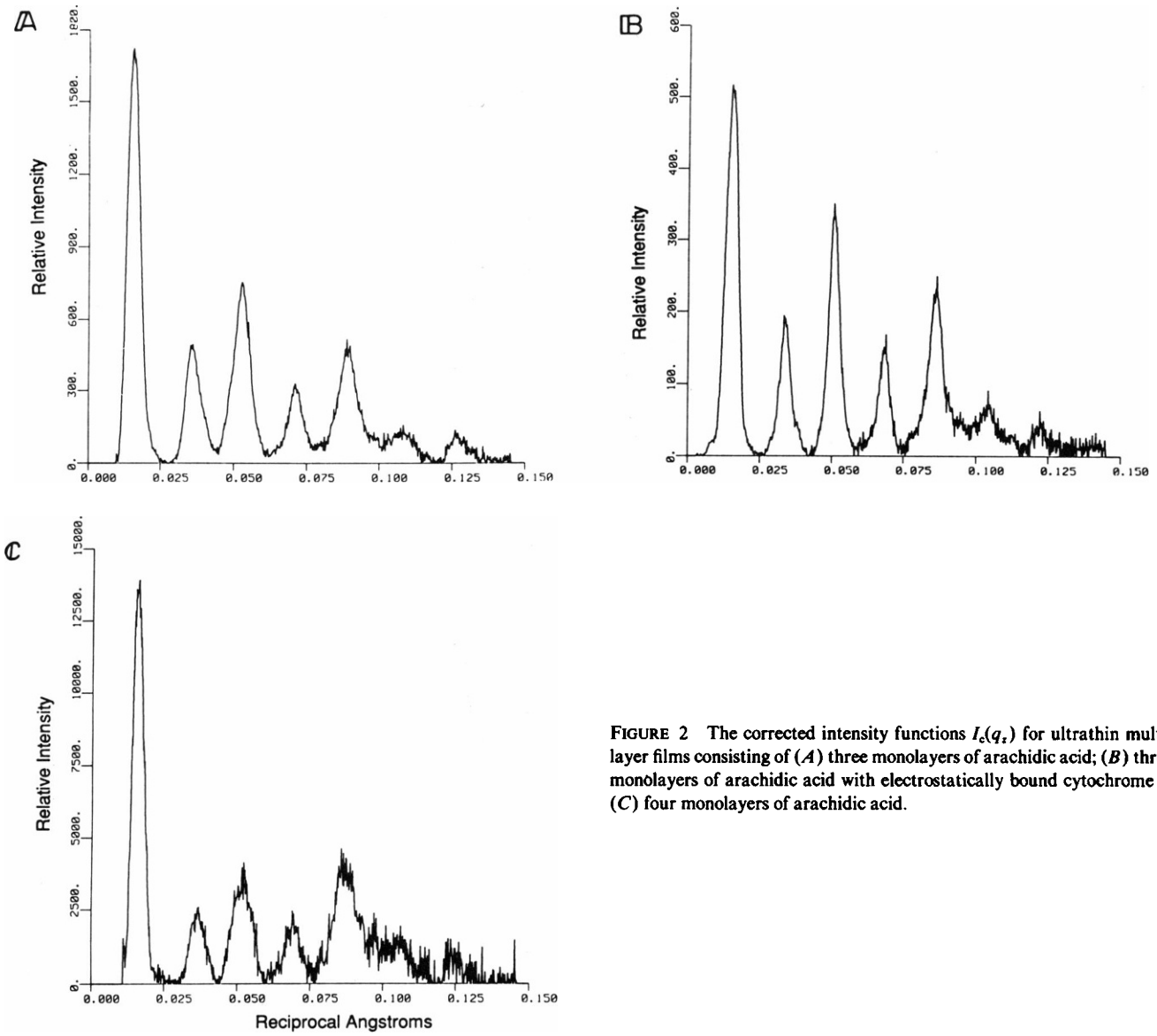

FIGURE 2 The corrected intensity functions $I_c(q_z)$ for ultrathin multilayer films consisting of (*A*) three monolayers of arachidic acid; (*B*) three monolayers of arachidic acid with electrostatically bound cytochrome *c*; (*C*) four monolayers of arachidic acid.

where D_n is the extent of the multilayer profile composed of n monolayers, so that $D_n = nd_0/2$. Small amplitude, low spatial frequency oscillations centered about the zero baseline extend beyond $\pm D_n$ due to the limited Δq_z resolution of the data and to errors in the corrected intensity function (dominated by errors in the background scattering correction at low q_z).

By comparing the autocorrelation functions calculated for the AAA multilayer (Fig. 4 *A*), the AAA w/cyto multilayer (Fig. 4 *B*), and the AAAA multilayer (Fig. 4 *C*), the effects of bound cytochrome *c* on the multilayer profile structure are indicated. The regions of the autocorrelation functions indicated over the range of the horizontal arrows are most sensitive to the presence or absence of bound cytochrome *c*; they are dominated by the correlations of the relative electron density profile features of the multilayer's first fatty acid monolayer on the alkylated glass substrate with the last surface fatty acid monolayer plus or minus cytochrome *c*. We note that significant differences exist (downward vertical arrows) within this region of the autocorrelation function for the AAA with cytochrome *c* multilayer (Fig. 4 *B*), which are absent in the comparable regions of the autocorrelation function for the AAA multilayer (Fig. 4 *A*) and the AAAA multilayer (Fig. 4 *C*). These same differences (denoted similarly by the arrows in Fig. 5) can be detected within the comparable regions of the autocorrelation functions for the AAAAA multilayer, the AAAAA w/cyto multilayer, and the AAAAAA multilayer (Fig. 5).

The inherently asymmetric profile structures of the ultrathin multilayer films used in this study (as evident from the corrected meridional intensity functions of Figs. 2 and 3) requires that the method used to determine the multilayer relative electron density profiles cannot assume

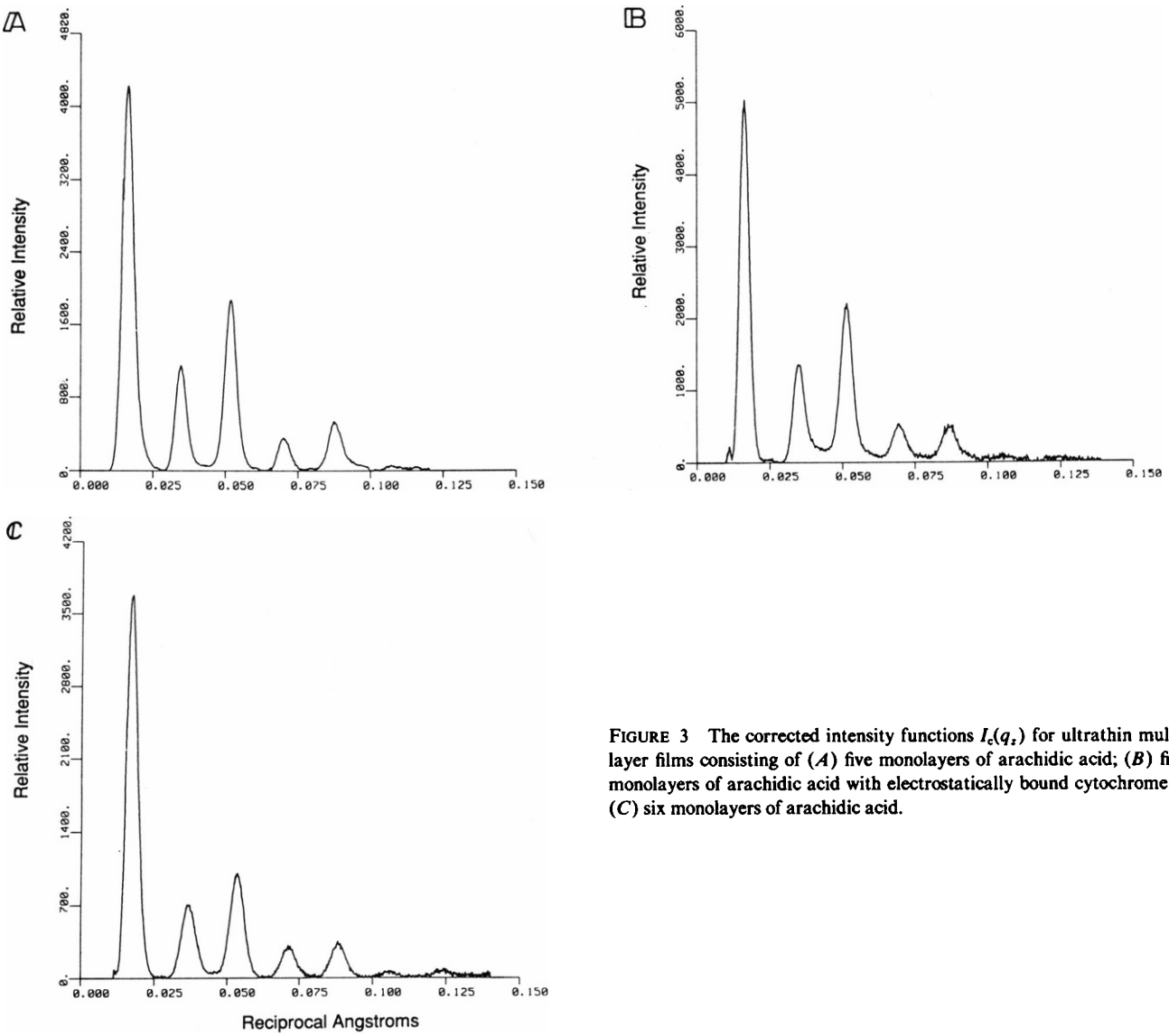

FIGURE 3 The corrected intensity functions $I_c(q_z)$ for ultrathin multilayer films consisting of (*A*) five monolayers of arachidic acid; (*B*) five monolayers of arachidic acid with electrostatically bound cytochrome *c*; (*C*) six monolayers of arachidic acid.

centrosymmetric phases. The box refinement procedure, which uses the simple boundary condition that the multilayer relative electron density profile structure is zero outside of a box of length D_n, has been effectively applied to meridional diffraction data from finite systems to produce correct multilayer profiles (14, 15, 17, 18). This technique is an iterative procedure that begins with the application of an arbitrary phase for each point in q_z, derived from the Fourier transform of some arbitrary trial function, to the modulus of the experimental structure factor, $[I_c(q_z)]^{1/2}$. A trial function such as a ramp function or a phase-shifted sinusoidal function will thus initiate the iteration with noncentrosymmetric phases.

However, the multilayer electron density profiles derived from the box refinement procedure are, to some extent, dependent on the trial function, and are not necessarily unique solutions. Various trial functions are therefore used to produce multilayer relative electron density profiles using the box refinement procedure; it has been previously found that the application of numerous arbitrary trial functions will lead to qualitatively similar multilayer profile structures (14, 15). For the results presented here, it was found that a number of arbitrary trial functions produced multilayer relative electron density profiles generally containing the expected features of fatty acid bilayer/monolayer profiles (e.g., electron deficient terminal methyl groups and electron dense carboxyl groups separated by dimensionally appropriate intermediate density methylene chain groups). In addition, these profiles have the proper number of monolayers, as independently verified by the multilayer profile autocorrelation functions.

Figs. 6 and 7 show the multilayer relative electron density profiles generated after 20 iterations by applying the box refinement method to the corrected intensity functions of Figs. 2 and 3, respectively. For these figures, the phase-shifted cosine trial function with an approximate wavelength of $D_n/2$ and the box used in applying the

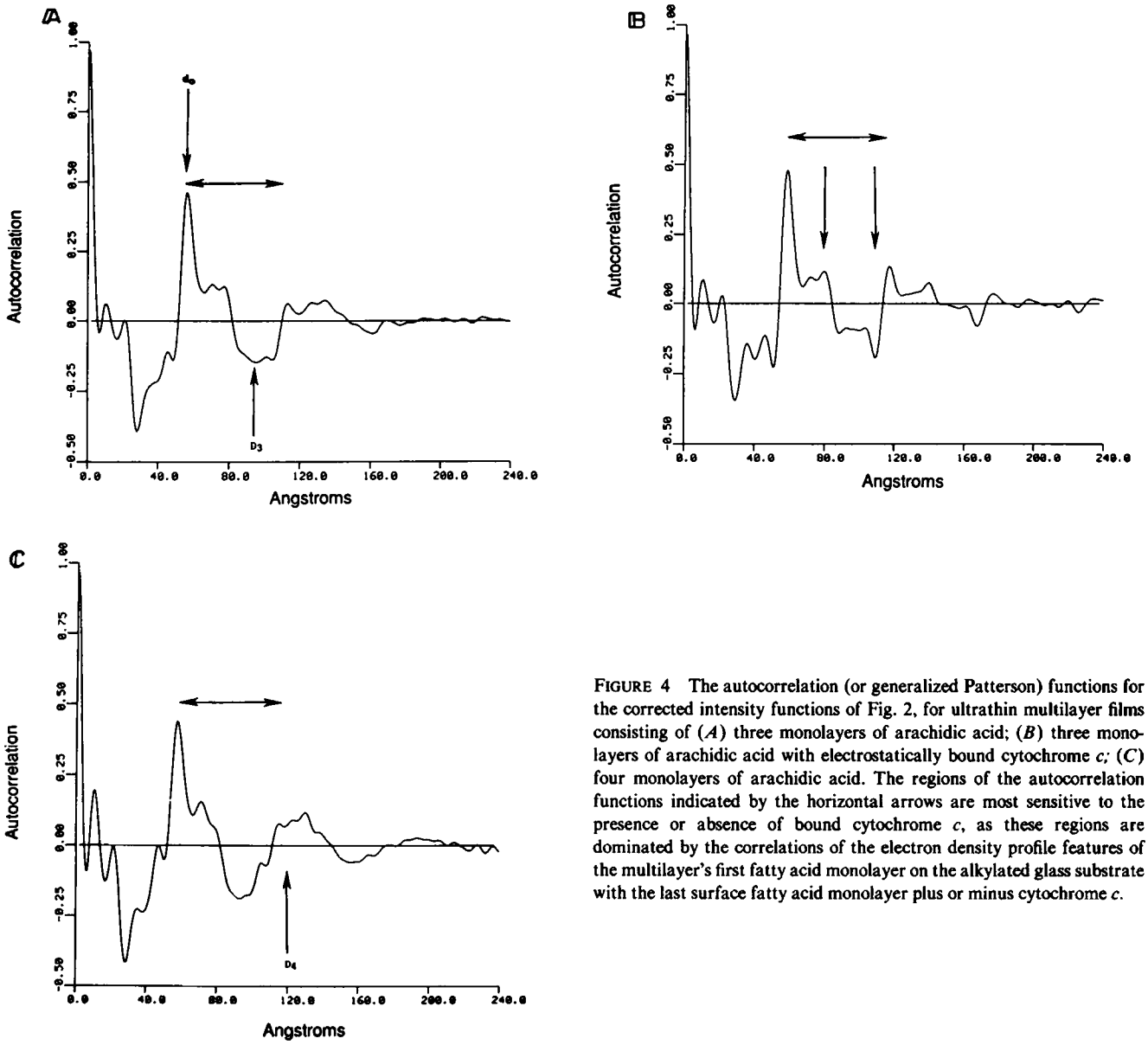

FIGURE 4 The autocorrelation (or generalized Patterson) functions for the corrected intensity functions of Fig. 2, for ultrathin multilayer films consisting of (*A*) three monolayers of arachidic acid; (*B*) three monolayers of arachidic acid with electrostatically bound cytochrome *c*; (*C*) four monolayers of arachidic acid. The regions of the autocorrelation functions indicated by the horizontal arrows are most sensitive to the presence or absence of bound cytochrome *c*, as these regions are dominated by the correlations of the electron density profile features of the multilayer's first fatty acid monolayer on the alkylated glass substrate with the last surface fatty acid monolayer plus or minus cytochrome *c*.

boundary constraint are shown. The relative electron density profiles for the AAA multilayer, AAA w/cyto multilayer, and AAAA multilayer were thus calculated using the same trial function and boundary constraint (Fig. 6). The major features common to all profiles include well-defined terminal methyl group troughs at $z \approx 0$ and 55 Å, while carboxyl group peaks appear at $z \approx 30$ and 85 Å. The carboxyl group peaks at $z \approx 85$ Å for the AAA multilayer and the AAA w/cyto multilayer appear somewhat disordered (broadened), and the AAA w/cyto multilayer has an additional strong peak at $z \approx 100$ Å (vertical arrows). This is in contrast to the sharper carboxyl group peak at $z \approx 85$ Å and the disordered terminal methyl group trough at $z \approx 100$ Å for the AAAA multilayer.

Similarly, the relative electron density profile for the AAAAA multilayer, AAAAA w/cyto multilayer, and AAAAAA multilayer are shown in Fig. 7. The major features common to all profiles include well-defined terminal methyl group troughs at $z \approx 0$, 55, and 110 Å, while carboxyl group peaks appear at $z \approx 30$, 85, and 140 Å. As in Fig. 6, the carboxyl group peaks at $z \approx 140$ Å for the AAAAA multilayer and the AAAAA w/cyto multilayer appear somewhat disordered (broadened), and the AAAAA w/cyto multilayer has an additional strong peak at $z \approx 150$ Å (vertical arrows). Again, in contrast, the AAAAAA multilayer has a sharper carboxyl group peak at $z \approx 140$ Å and a disordered terminal methyl trough at $z \approx 165$ Å.

We note that each of the two sets of multilayer relative electron density profiles presented in Figs. 6 and 7 represents a "homologous series" of multilayer structures (see references 14 and 15). In addition, the pairs of multilayer relative electron density profiles for AAA and AAAAA, AAA w/cyto and AAAAA w/cyto, AAAA and

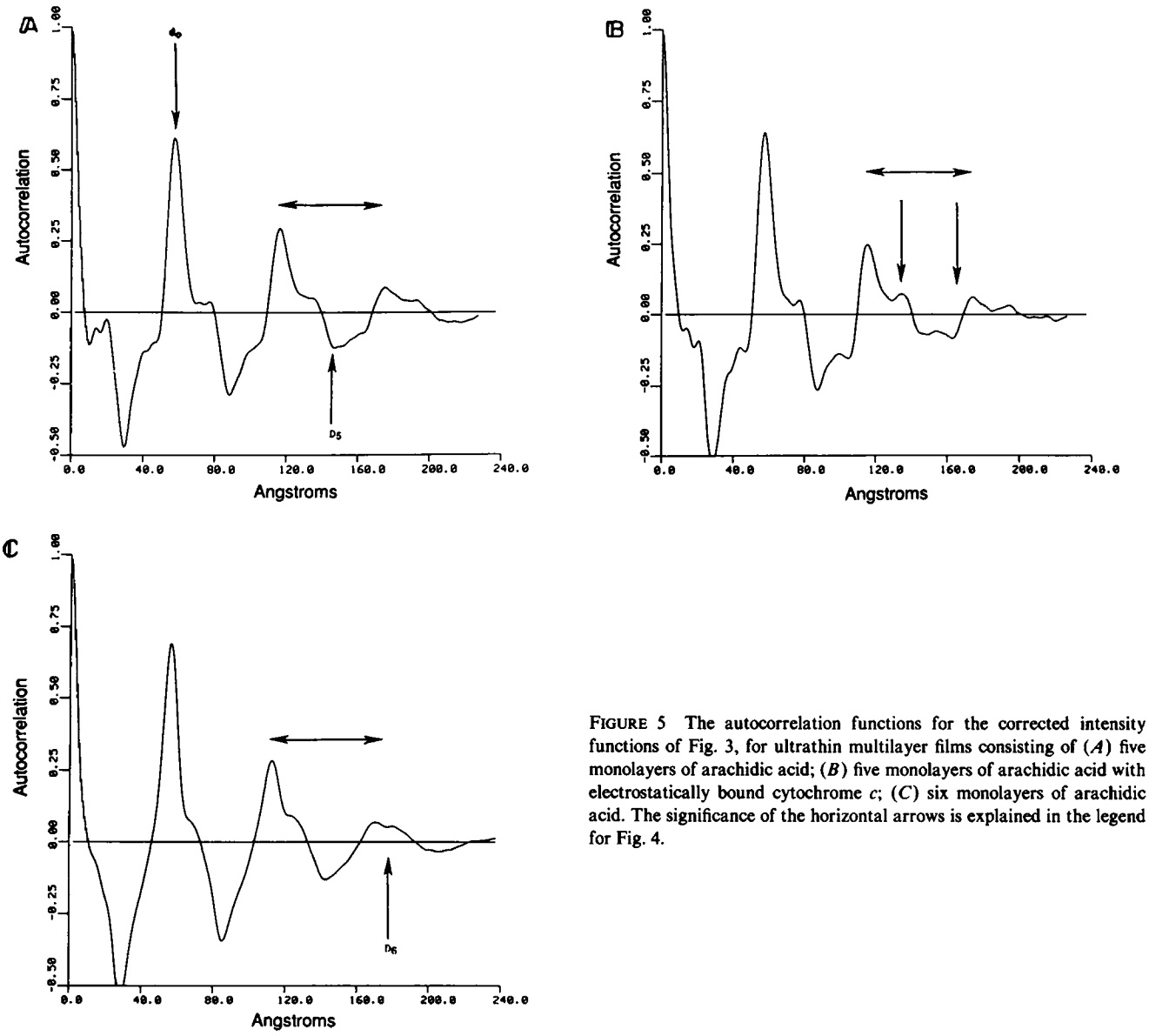

FIGURE 5 The autocorrelation functions for the corrected intensity functions of Fig. 3, for ultrathin multilayer films consisting of (*A*) five monolayers of arachidic acid; (*B*) five monolayers of arachidic acid with electrostatically bound cytochrome *c*; (*C*) six monolayers of arachidic acid. The significance of the horizontal arrows is explained in the legend for Fig. 4.

AAAAAA also each represent a "homologous series" of multilayer structures. The overall considerable similarities of major features among the various multilayer electron density profiles within these various "homologous series" strongly indicate the correctness of the phase solutions achieved via the independent application of the box refinement method to the meridional intensity functions for the various nonperiodic multilayers investigated. We note that references 14 and 15 and the submissions listed in footnotes 1 and 3 contain many detailed examples of the use of the box-refinement method for the determination of a variety of nonperiodic and near-periodic ultrathin lipid multilayer profiles. For the latter cases, comparisons with Patterson function deconvolution methods using centrosymmetric phases are also presented. In addition, we have recently used heavy-atom substitution and resonance x-ray diffraction methods to further verify the correctness of the phase solutions achieved via the box-refinement method for such nonperiodic lipid multilayers.[2]

DISCUSSION

Cytochrome *c* has been previously found to cause a significant change in surface pressure of a monolayer of steric acid at an air–water interface, which was shown to be a result of the protein binding to the lipid film (10). In the present study, cytochrome *c* was reacted with the surface of ultrathin multilayer films under conditions that would promote protein binding to the surface (low ionic strength, at pH 8 whereby the fatty acid carboxyl group retains a negative charge and the protein a net positive charge). Thus, cytochrome *c* was found to bind to arachidic acid multilayer films having three and five monolayers of lipid (having a hydrophilic carboxyl group surface); the protein did not bind to glass substrates, nor to films having four

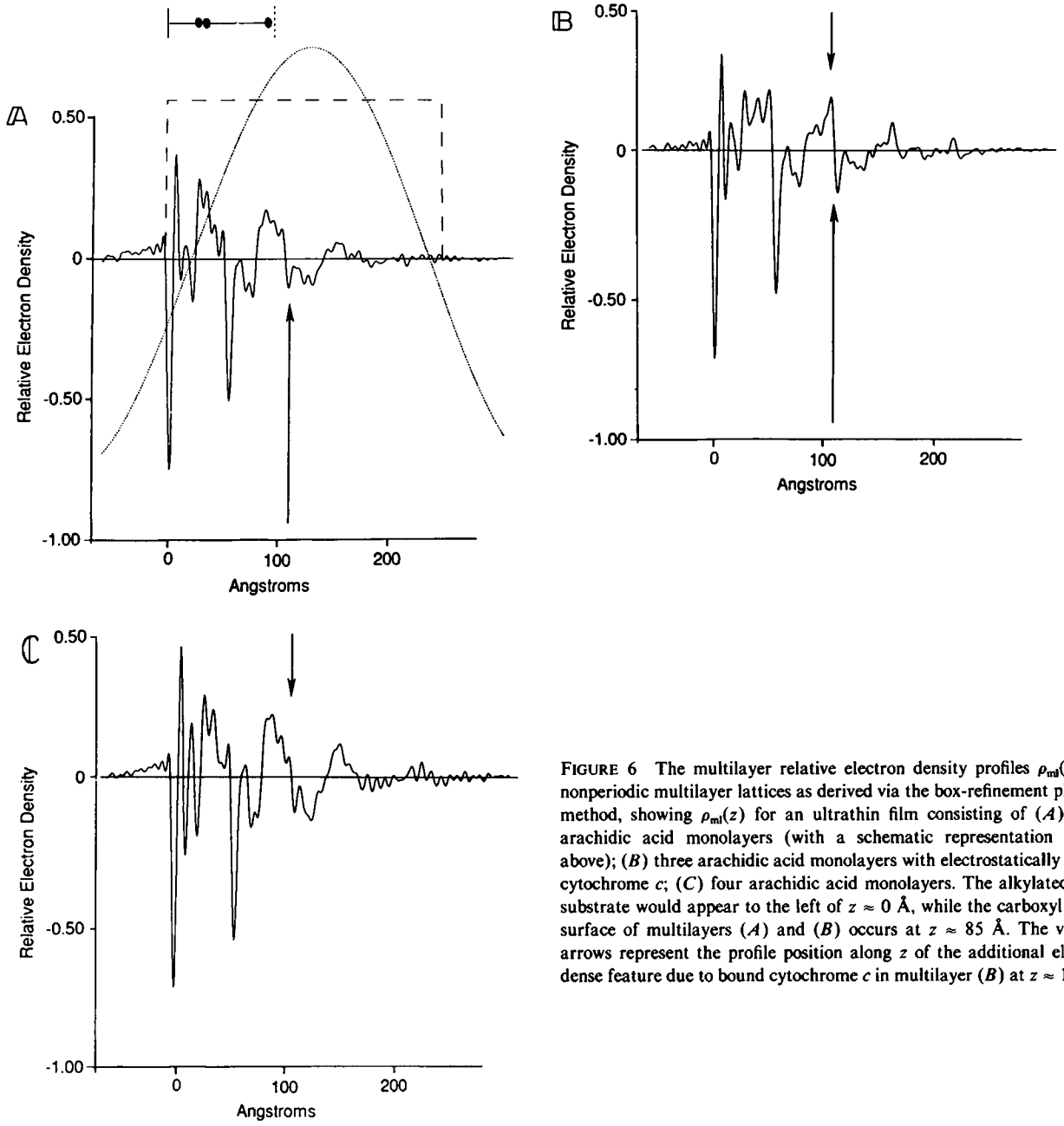

FIGURE 6 The multilayer relative electron density profiles $\rho_{ml}(z)$ for nonperiodic multilayer lattices as derived via the box-refinement phasing method, showing $\rho_{ml}(z)$ for an ultrathin film consisting of (*A*) three arachidic acid monolayers (with a schematic representation shown above); (*B*) three arachidic acid monolayers with electrostatically bound cytochrome *c*; (*C*) four arachidic acid monolayers. The alkylated glass substrate would appear to the left of $z \approx 0$ Å, while the carboxyl group surface of multilayers (*A*) and (*B*) occurs at $z \approx 85$ Å. The vertical arrows represent the profile position along *z* of the additional electron dense feature due to bound cytochrome *c* in multilayer (*B*) at $z \approx 100$ Å.

and six monolayers (having a hydrophobic methyl group surface). The experimentally determined amount of bound protein was within the expected value for a hexagonal close-packed monolayer of cytochrome *c* on the multilayer film surface. It was also found that the amount of cytochrome *c* bound to such ultrathin multilayer films with a surface monolayer of phosphatidyl inositol (having a greater net negative charge) was the equivalent (within experimental error) to the amount of protein bound to arachidic acid film surface (data not shown).

It is well-established that cytochrome *c* binding to lipid monolayers and bilayers is highly dependent on the effective lipid charge, as determined by the experiments varying ionic strength and pH (9). As expected, cytochrome *c* binding to the surface of arachidic acid films having three or five monolayers is also highly dependent on ionic strength, since cytochrome *c* was removed from the surface when the films were incubated in a buffer containing 0.1 M KCl. Decreasing amounts of protein were released from the films when they were incubated with buffers containing 0.01 M KCl and 0.001 M KCl (data not shown). Although the binding of cytochrome *c* to anionic lipids is a relatively nonspecific electrostatic interaction, we have demonstrated in related experiments (Pachence, J. M., J. Vanderkoii, P. L. Dutton, and J. K. Blasie, unpublished data) that the lateral motion of the protein is highly restricted in the plane of the multilayer surface (as indicated from the protein diffusion constant derived from

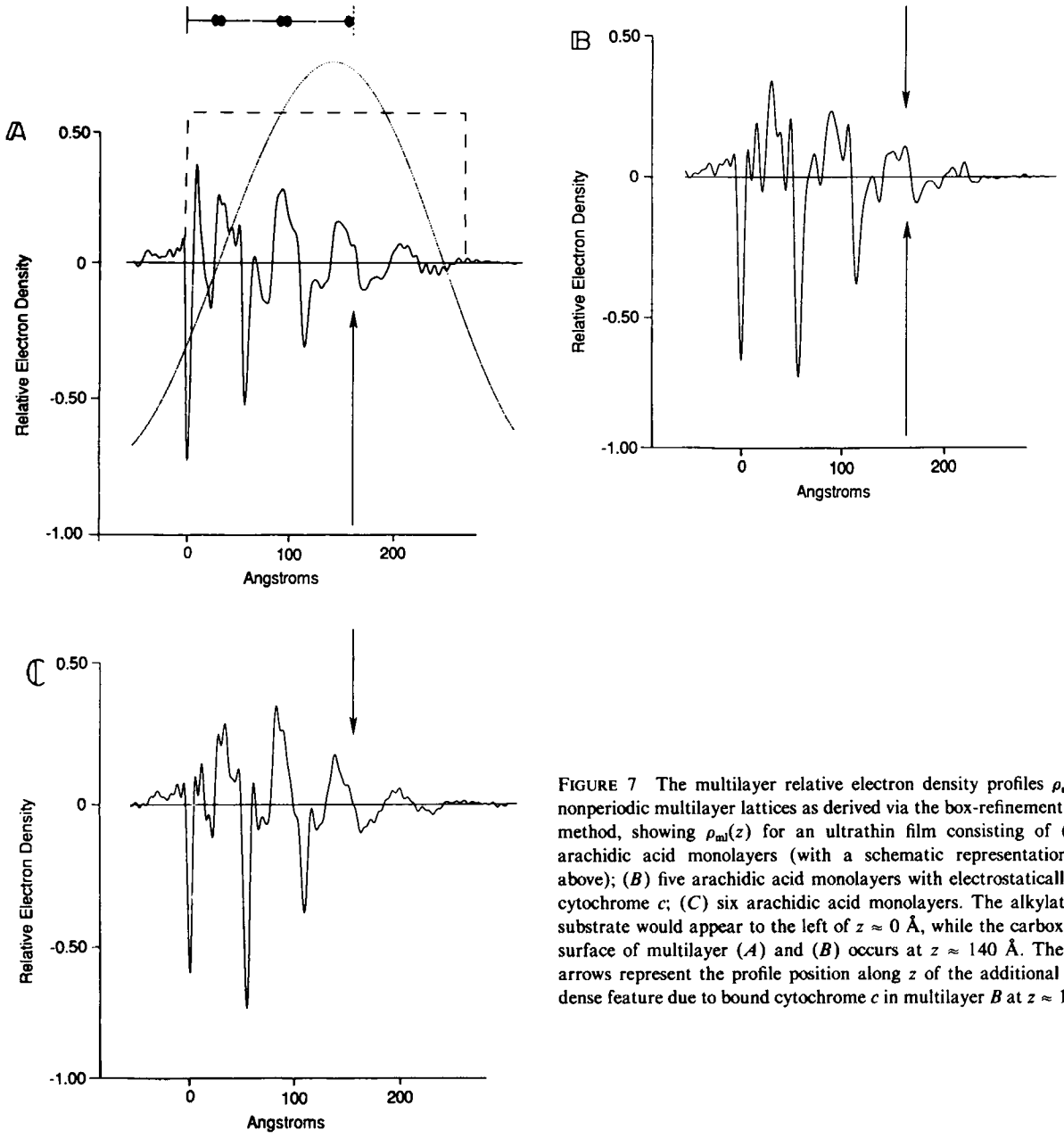

FIGURE 7 The multilayer relative electron density profiles $\rho_{rel}(z)$ for nonperiodic multilayer lattices as derived via the box-refinement phasing method, showing $\rho_{rel}(z)$ for an ultrathin film consisting of (*A*) five arachidic acid monolayers (with a schematic representation shown above); (*B*) five arachidic acid monolayers with electrostatically bound cytochrome *c*; (*C*) six arachidic acid monolayers. The alkylated glass substrate would appear to the left of $z \approx 0$ Å, while the carboxyl group surface of multilayer (*A*) and (*B*) occurs at $z \approx 140$ Å. The vertical arrows represent the profile position along *z* of the additional electron dense feature due to bound cytochrome *c* in multilayer *B* at $z \approx 150$ Å.

fluorescence recovery after photobleaching [FRAP] experiments), and that the protein has a high degree of orientation relative to the multilayer surface (as indicated from the tilt of its heme group with respect to the plane of the multilayer surface, as derived from optical linear dichroism experiments).

Significant changes occurred in the corrected meridional intensity data for the ultrathin multilayer films with bound cytochrome *c* (Figs. 2 and 3). These changes are reflected in the multilayer profile autocorrelation functions of Figs. 4 and 5, and in the multilayer relative electron density profiles of Figs. 6 and 7. Autocorrelation functions for multilayer relative electron density profiles with a finite number of monolayers are essentially zero for $|z| > nd_0/2 = D_n$, where n is the number of monolayers and d_0 is the profile length in z of an average bilayer. As can be seen, the autocorrelation functions for the ultrathin films AAA (Fig. 4 *A*) and AAAAA (Fig. 5 *A*) are dominated by only negative correlations for $|z| \approx D_3$ and $|z| \approx D_5$, respectively. This is due primarily to the correlation of the negative electron deficient terminal methyl group feature at the multilayer–substrate interface with the positive electron dense carboxyl group feature at the multilayer–air interface in such multilayer electron density profiles (see references 14 and 15). Fig. 4 *B* (AAA w/cyto) and Fig. 5 *B* (AAAAA w/cyto) have these same negative correlations, except that an additional strong negative feature appears for $D_3 \leq |z| \leq D_4$ and $D_5 \leq |z| \leq D_6$, respectively. This feature indicates that an additional electron dense feature appears on the multilayer–air surface at larger $|z|$ due to

the addition of bound cytochrome *c*. Addition of another monolayer of lipid to an odd-number monolayer multilayer (producing AAAA or AAAAAA) leads to positive correlations at $|z| \approx D_4$ and $|z| \approx D_6$, as expected. This is due primarily to the correlation of the resulting negative electron deficient terminal methyl group features at both multilayer surfaces in such multilayer relative electron profiles (see references 14 and 15). These characteristics noted for the multilayer profile autocorrelation functions are significant, as they clearly demonstrate appropriate structural changes in the surface layer of the ultrathin multilayer films used in this study. Hence, these autocorrelation functions (which are independent of phase information) can be used in support of the changes seen in the multilayer relative electron density profile structures, which are functions dependent on applying correct phase information.

By comparing the major features of the multilayer relative electron density profiles with and without cytochrome *c* in Figs. 6 and 7, it can be seen that an additional strong positive electron density feature appears at one surface of the multilayer profiles containing bound protein (Figs. 6 *B* and 7 *B*). Note that the profile *z*-position of this additional electron dense feature corresponds to the downward slope of the carboxyl group peak for multilayers with an odd number of monolayers (Figs. 6 *A* and 7 *A*), and to the disordered terminal methyl group trough for multilayers with an even number of monolayers (Figs. 6 *C* and 7 *C*). In general, the effect of the bound protein on the one surface of the multilayer relative electron profile is independent of the number of fatty acid monolayers (compare Figs. 6 *B* and 7 *B*).

In a previous investigation on the structure of ultrathin fatty acid multilayer films, it was found that one monolayer at one edge of the multilayer profile was disordered (14). This study proved that the disordered monolayer occurred on the multilayer surface, namely at the air–multilayer interface (15). The assignment of the air–multilayer interface versus the octadecyltrichlorosilane (OTS)–multilayer interface in accordance with our previous study is useful in interpreting the multilayer profile structures with and without bound cytochrome *c* presented in Figs. 6 and 7 (14, 15). As can be seen in Figs. 6 and 7, each relative electron density profile begins with a well-defined terminal methyl group trough, which is thereby presumed to be at the OTS–multilayer interface. As expected from our previous results, the carboxyl group electron density peaks at the outer (air) surface of multilayer profiles for the odd-numbered monolayer films have a larger width than the interior-layer carboxyl peaks (Figs. 6 *A* and 7 *A*). Likewise, the terminal methyl group troughs at the outer (air) surface of the multilayer profiles for the even numbered monolayer films have a larger width than the interior-layer terminal methyl troughs (Figs. 6 *C* and 7 *C*). Consequently, the additional strong electron dense feature appearing for the multilayer profiles containing cytochrome *c* (Figs. 6 *B* and 7 *B*) occurs on the outer (air) surface of the multilayer.

It appears from the multilayer profiles containing cytochrome *c* that the width of this additional electron dense feature on the multilayer surface is substantially <25 Å, the smallest diameter of horse heart cytochrome *c* (19). Although this electron dense feature in the profiles of Figs.

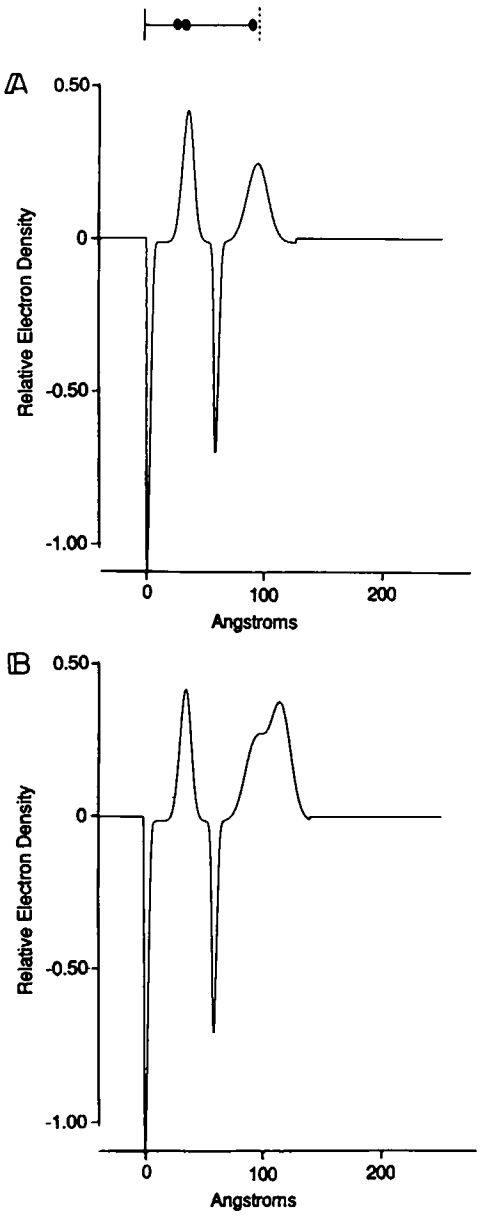

FIGURE 8 (*A*) A relative electron density profile for a model three monolayer fatty acid multilayer, using four Gaussian functions. The profile positions and initial widths of the Gaussians were determined from the experimental electron density profile of Fig. 6 *A*. (*B*) A relative electron density profile for a model three monolayer fatty acid multilayer with bound cytochrome *c*; a fifth Gaussian was added to the model shown in *A*. The profile position and width of this additional Gaussian feature was determined by qualitatively comparing the square of the Fourier transform modulus of the model with the experimental corrected intensity function of Fig. 2 *B*.

6 *B* and 7 *B* is not completely resolved from the neighboring carboxyl group peak, the width of this feature is estimated to be half that expected for cytochrome *c*. To assist in the interpretation of the cytochrome *c* location in the multilayer profiles, a model calculation was used. A model three-monolayer profile consisting of Gaussian functions located at the terminal methyl group troughs and the carboxyl group peaks of the multilayer relative electron density profile of Fig. 6 *A* was constructed (Fig. 8 *A*). The widths of the Gaussian functions were varied until the general characteristics of the corrected meridional intensity function for three monolayers (Fig. 2 *A*) were well reproduced via the Fourier transform modulus squared of the model multilayer profile structure. Subsequently, a peak of electron density of varying widths and profile *z*-positions was added to the outer surface of this model

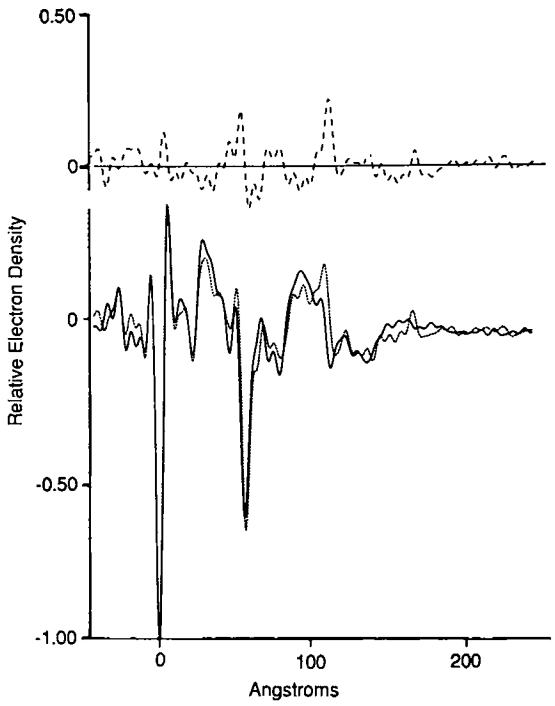

FIGURE 9 (*A*) The relative electron density profile of the three monolayer arachidic acid multilayer obtained via box-refinement using the model multilayer profile of Fig. 8 *A* as the trial structure (*solid line*). (*B*) The relative electron density profile of the three monolayer arachidic acid multilayer with electrostatically bound cytochrome *c* using the same model multilayer profile of Fig. 8 *A* as the trial structure (*dotted line*). The difference profile (9 *B* minus 9 *A*, *dashed line*) clearly indicates that the only pronounced difference between these two multilayer profiles is due to the additional strong cytochrome *c* feature occurring at the air–surface of the three monolayer fatty acid multilayer ($z \approx 100$ Å), while the expected typical features[4] of the underlying fatty acid multilayer are nearly identical for the two multilayer profiles (i.e., slightly shifted terminal methyl group troughs at $z \approx 0$ and 55 Å and carboxyl group peaks at $z \approx 30$ and 85 Å separated by dimensionally appropriate regions of nearly uniform intermediate density methylene chains). Note that the "overshoot" about the sharp terminal methyl group trough at $z \geq 0$ Å arises from small errors in the background scattering correction (see reference 14 for details).

three-monolayer profile, and these so-modified model multilayer profiles were Fourier transformed to produce a calculated meridional intensity function. To reproduce a calculated intensity function with the proper general characteristics of the experimental corrected meridional intensity function of Fig. 2 *B*, it was necessary to add an electron dense peak of 20-Å width overlapping the outer carboxyl group peak of the model three monolayer profile, as shown in Fig. 8 *B*.

It is important to note that in the analysis of less than perfect meridional diffraction data from ultrathin, nonperiodic multilayers (in terms of Δq_z resolution, counting statistics, etc.) via the box-refinement method, the quality of the derived multilayer electron density profiles can be substantially improved by using trial profile structures more similar to the anticipated multilayer profile structures as compared with those derived using totally arbitrary trial structures (14, 18)[1] described in the Results section. To investigate the effects of such imperfections in the diffraction date on the derived multilayer electron density profiles shown in Figs. 6 and 7, we used for example the model multilayer profile of Fig. 8 *A* as the trial profile structure in the box-refinement of both the meridional intensity functions of Fig. 2, *A* and *B* for the three-monolayer arachidic acid multilayers without and with cytochrome *c*, respectively. The resulting multilayer electron density profiles are shown in Fig. 9, *A* and *B* respectively. The pronounced additional electron dense feature on the air–surface of the three-monolayer multilayer profile ascribed to cytochrome *c* distinctly reappears as expected at $z \sim 100$ Å in Fig. 9 *B* while the features within the profile of the underlying arachidic acid multilayer in Fig. 9, *A* and *B* are nearly identical and relatively smooth, fully consistent with the expected profile projection of such an ultrathin fatty acid multilayer structure[4] (e.g., terminal methyl group troughs at $z \sim 0$ Å and ~55 Å and carboxyl group peaks at $z \sim 30$ Å and ~85 Å separated by dimensionally appropriate regions of nearly uniform intermediate density methylene chains). In addition, the features in both multilayer profiles of Fig. 9, *A* and *B* beyond either surface of the multilayer profiles ($z < 0$ Å and $z > 110$ Å) are relatively smooth even though they occur inside the box constraint. Since both the multilayer profiles of Figs. 9 *A* and 6 *A* and of Figs. 9 *B* and 6 *B* match their respective meridional intensity functions of Fig. 2, *A* and *B* (and their Fourier transforms, i.e., the

[4]We note that the significance of the shapes, relative positions, etc. of the typical features within the relative electron density profiles of nonperiodic and near-periodic, ultrathin multilayers of amphiphilic molecules as derived via the box-refinement method have been extensively investigated in references 14 and 15 and submissions in footnotes 1–3. For the near-periodic, ultrathin multilayers, comparisons of these typical features with those contained within the average bilayer profile (as derived via a Patterson function deconvolution method using centrosymmetric phases) have been analyzed.

multilayer profile autocorrelation functions of Fig. 4, *A* and *B*, respectively) to within the counting statistics, the differences between the multilayer profiles of Fig. 9 *A* vs. 6 *A* and Fig. 9 *B* vs. 6 *B* must arise from the above-mentioned imperfections in the experimental intensity functions. The multilayer profiles shown in Fig. 9 for example represent therefore the best profiles achievable via the box-refinement phasing method with the meridional diffraction data used.[5]

Under conditions where cytochrome *c* would electrostatically bind to an anionic lipid, other investigators have shown that cytochrome *c* causes significant surface pressure changes for anionic lipid films (e.g., references 10–12). Such surface pressure changes have been interpreted as resulting from some degree of penetration of the protein into the lipid hydrocarbon chain region of the monolayer (10–12). Although earlier x-ray diffraction studies of cytochrome *c*/lipid systems using dispersions of multilamellar vesicles have supported this interpretation (20), the present study has provided structural results concerning the interaction of cytochrome *c* with a single, extended surface monolayer of lipid. The above model calculations are helpful in interpreting otherwise complex electron density profiles of lipid/protein complexes (e.g., 2, 8) and indicate that the cytochrome *c* monolayer penetrates the hydrophilic lipid carboxyl group surface to the level of the hydrocarbon chains. However, other powerful diffraction methods may need to be used to more precisely locate cytochrome *c* in the multilayer profiles of Figs. 6 *B* and 7 *B* and determine the effect of cytochrome *c* binding on the underlying lipid bilayer structure. Recent results suggest that both neutron diffraction and resonance x-ray diffraction can be used to uniquely determine the separate protein and lipid contributions to the profile structures of such ultrathin multilayer films with a surface monolayer of cytochrome *c*, in a manner analogous to that previously used for thick membrane multilayers (2, 3, 8).

CONCLUSION

The multilayer electron density profiles (and their autocorrelation functions) derived for the various nonperiodic ultrathin multilayer films investigated in this structural study are clearly of sufficient quality to firmly establish the presence of a cytochrome *c* monolayer electrostatically bound to the surface of fatty acid multilayers containing an odd number of monolayers. The quality of such electron density profiles for such nonperiodic ultrathin multilayers can be improved substantially by using synchrotron radiation to achieve enhanced Δq_z resolution, spatial resolution, and counting statistics.[1] In addition, neutron diffraction coupled with specific deuteration of selected multilayer components can uniquely determine the separate contributions of lipid and protein to the nonperiodic multilayer profile structure. Nevertheless, the preliminary structural studies reported here (using a relatively small protein) strongly suggest that diffraction methods can be used to accurately monitor the fabrication of vectorially oriented macromolecular assemblies on the surface of nonperiodic ultrathin multilayer films with macroscopic in-plane dimensions. In particular, we plan to next use cytochrome *c* covalently bound to the surface of such ultrathin multilayer films to assemble functional complexes of cytochrome *c* with cytochrome oxidase, cytochrome b/c_1, and photosynthetic reaction center protein.

This work was supported by the National Institutes of Health grant No. GM-33525.

Received for publication 9 March 1987 and in final form 29 June 1987.

[5]By using a trial structure of the appropriate model multilayer electron density profiles for the underlying fatty acid multilayers (as shown in Fig. 8 *A*, for instance) in the box-refinement analysis, meridional diffraction data from the multilayers having the same number of monolayers plus a surface layer of protein are thus phased in a way that is analogous to phasing diffraction data via the more powerful method of interferometry (see especially reference 21). However, the refinement approach allows the possibility of variation of the underlying fatty acid multilayer structure in the presence of the protein surface layer, unlike the more strict interferometry method (see Fig. 9 legend).

REFERENCES

1. Pachence, J. M., P. L. Dutton, and J. K. Blasie. 1979. Structural studies on reconstituted reaction center-lipid membranes. *Biochim. Biophys. Acta.* 548:348–373.
2. Pachence, J. M., P. L. Dutton, and J. K. Blasie. 1983. A structural investigation of cytochrome *c* binding to photosynthetic reaction centers in reconstituted membranes. *Biochim. Biophys. Acta.* 724:6–19.
3. Blasie, J. K., J. M. Pachence, A. Tavormina, P. L. Dutton, J. Stamatoff, P. Eisenberger, and G. Brown. 1983. The location of redox centers in the profile structure of a reconstituted membrane containing a photosynthetic reaction center-cytochrome *c* complex by resonance x-ray diffraction. *Biochim. Biophys. Acta.* 723:350–357.
4. Deisenhofer, J., O. Epp, K. Miki, R. Huber, and H. Michel. 1984. Structure of the protein subunits in the photosynthetic reaction centre of *Rhodopseudomonas viridis* at 3 Å resolution. *Nature (Lond.).* 318:618–624.
5. Blasie, J. K., M. Erecinska, S. Samuels, and J. S. Leigh. 1978. The structure of a cytochrome oxidase-lipid model membrane. *Biochim. Biophys. Acta.* 501:33–53.
6. Packam, N. K., P. L. Dutton, and P. Mueller. 1982. Photoelectric currents across planar bilayer membranes containing bacterial reaction centers. *Biophys. J.* 37:465–473.
7. Montal, M., and P. Mueller. 1972. Formation of biomolecular membranes from lipid monolayers and a study of their electrical properties. *Proc. Natl. Acad. Sci. USA.* 69:3561–3566.
8. Pachence, J. M., P. L. Dutton, and J. K. Blasie. 1981. The reaction center profile structure derived from neutron diffraction. *Biochim. Biophys. Acta.* 635:267–283.
9. Nicholls, P. 1974. Cytochrome *c* binding to enzymes and membranes. *Biochim. Biophys. Acta.* 346:261–310.
10. Quinn, P. J., and R. M. C. Dawson. 1969. Interactions of cytochrome *c* and C^{14}-carboxymethlated cytochrome *c* with monolayers of phosphatidylcholine, phosphatidic acid, and cardiolipin. *Biochem. J.* 115:65–75.

11. Morse, P. D., and D. W. Deamer. 1973. Interaction of cytochrome *c* with lipid monolayers. *Biochim. Biophys. Acta.* 298:769–782.

12. Steinemann, A., and P. Lauger. 1971. Interaction of cytochrome *c* with phospholipid monolayers and bilayer membranes. *J. Membr. Biol.* 4:74–86.

13. Garito, A. F., K. D. Singer, and C. C. Teng. 1983. Organic crystals and polymers. A new class of non-linear optical materials. *In* Nonlinear Optical Properties of Organic Polymer Materials. D. Williams, editor. ACS Symp. 223.

14. Skita, V., M. Filipkowski, A. F. Garito, and J. K. Blasie. 1986. Profile structures of very thin multilayers by x-ray diffraction using direct and refinement methods of analysis. *Phys. Rev. B* 34:5826–5837.

15. Skita, V., W. Richardson, M. Filipkowski, A. F. Garito, and J. K. Blasie. 1987. Overlayer-induced ordering of the disordered surface monolayer in Langmuir-Blodgett thin films. *J. Physique.* 47:1849–1855.

16. Sagiv, J. 1980. Organized monolayers by adsorption. I. Formation and structure of oleophobic mixed monolayers on solid surfaces. *J. Am. Chem. Soc.* 102:92–98.

17. Stroud, R. M., and D. A. Agard. 1979. Structure determination of asymmetric membrane profiles using an iterative Fourier method. *Biophys. J.* 25:495–514.

18. Makowski, L. 1981. The use of continuous diffraction data as a phase constraint. I. One-dimensional theory. *J. Appl. Cryst.* 14:734–742.

19. Dickerson, R. E., and R. Timkovich. 1975. Cytochromes *c*. *In* The Enzymes. 3rd ed. Vol. 11. P. D. Boyer, editor. Chapt. 7. Academic Press, Inc., New York. 395–544.

20. Shipley, G. G., R. B. Leslie, and D. Chapman. 1969. X-ray diffraction study of the interaction of phospholipids with cytochrome *c* in the aqueous phase. *Nature (Lond.).* 222:561–562.

21. Lesslauer, W., and J. K. Blasie. 1971. X-ray holographic interferometry in the determination of planar multilayer structures. Theory and experimental observations. *Acta Crystallogr.* A27:456–461.